

# Modelling and Simulation of an Aerosol-on-Demand Print Head with Computational Fluid Dynamics

Martin Ungerer<sup>1</sup>, David Zeltner<sup>1</sup>, Achim Wenka<sup>2</sup>, Ulrich Gengenbach<sup>1</sup><sup>a</sup> and Ingo Sieber<sup>1</sup><sup>b</sup>

<sup>1</sup>*Institute for Automation and Applied Informatics, KIT, Hermann-von-Helmholtz-Platz1, 76344 Egg.-Leo, Germany*

<sup>2</sup>*Institute for Micro Process Engineering, KIT, Hermann-von-Helmholtz-Platz1, 76344 Egg.-Leo, Germany*

**Keywords:** Computational Fluid Dynamics, Modelling, Simulation, Additive Manufacturing.

**Abstract:** In this paper we present the functional validation of a newly developed concept of a print head for aerosol-on-demand printing using fluid dynamical modelling and simulation. In our concept of the aerosol-on-demand print head, the ink is atomised by ultrasonic excitation and focussed by a sheath gas in a converging nozzle. The special feature of this new concept is aerosol generation directly in the print head thus allowing for on-demand operation. Using computational fluid dynamics (CFD), a pre-manufacturing study is being carried out to validate the operation of the concept as well as to find a design-for-manufacture.

## 1 INTRODUCTION

Novel devices and systems with special chemical, physical or optical properties can be realised by printing processes using functionalized inks (Sirringhaus and Shimoda 2003; Sieber, Thelen, and Gengenbach 2020, 2021; Magdassi 2010). Drop-on-demand inkjet printing has achieved a high level of development in printing functional structures (Sirringhaus and Shimoda 2003). In contrast to drop-on-demand inkjet printing, aerosol jet printing has the advantages of potentially printing finer structures with higher resolution and the capability to print on three dimensional structures (Mette et al. 2007, Neotech 2021), or even bond multiple chip layer together, thus replacing the need for wire bonding (Hedges and Marin 2012).

Aerosol jet printing is a continuous printing process where a fine spray of atomised ink is focussed hydrodynamically by means of a sheath gas flow. This results in a stable, and over a range of several millimetres well-collimated aerosol jet (Ganz et al. 2016; Gupta et al. 2016). A currently unsolved problem in aerosol jet printing is, that it cannot be operated in on-demand mode. This is because a run-in time of the aerosol generation is required, since in current aerosol jet printers the generation of the aerosol takes place in an atomisation unit which is

detached from the nozzle. Thus, switching the jet generation on and off for on-demand operation is not possible (Chang, Facchetti, and Reuss 2017; Hedges and Marin 2012).

To address this point we develop a new principle for an aerosol jet-on-demand (AoD) print head (Ungerer et al. 2018). Centerpiece of this concept is the integration of the atomisation unit into the print head. The aerosol is generated by means of ultrasonic atomisation of the ink in the capillary with the aid of a piezo actuator. Aerodynamical focusing of the aerosol jet is based on the sheath gas mass flow, the aerosol mass flow and the outlet nozzle. Thus, a compact system design can be developed which will allow for printing operation in all spatial directions, a widely tunable nozzle-to-substrate distance, as well as a jet-on-demand mode of operation (Ungerer 2020; Sieber et al. 2022).

This paper will focus on the proof-of-concept based on CFD simulations. In the simulations the functional ink is modelled as distilled water. This is justified, since the aerodynamic focusing is independent of the dynamic viscosity of the fluid or the particle content in the fluid. Hence, an aerodynamic focusing of all fluids that can be atomised in the capillary is possible. For modelling of the print head the limitations of the manufacturing processes used (design-for-manufacturing) are taken

<sup>a</sup> <https://orcid.org/0000-0001-9762-0019>

<sup>b</sup> <https://orcid.org/0000-0003-2811-7852>

into account. The organisation of this paper is as follows: Section 2 addresses the design-for-manufacturing of a laboratory setup of the print head. In Section 3, modelling of the print head is presented. Herein a brief theoretical description of the used model approach is presented as well as the geometry model and the meshing. Simulation and its results are presented in Section 4, the paper concludes with a discussion of the results and a brief outlook in Section 5.

## 2 DESIGN-FOR-MANUFACTURING

Fig. 1 shows the schematic of the principle design of the inner contour of the aerosol print head. The aerosol is generated by ultrasonic atomisation of the ink in the capillary with the aid of a piezo actuator. The tip of the capillary is located in a rotationally symmetric chamber, the mixing chamber, into which a sheath gas is injected to aerodynamically focus the atomised ink in the nozzle.

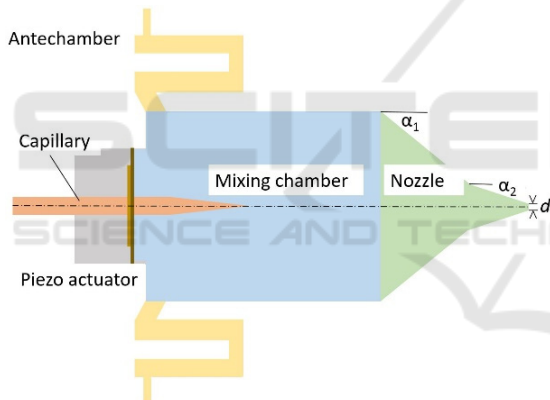


Figure 1: Schematic of the principle design.

In order to obtain a uniform, rotationally symmetric aerosol jet, a uniform flow of the sheath gas around the capillary is necessary. To achieve this, the velocity profile of the sheath gas, which flows in from four inlets evenly distributed around the circumference, is homogenised in a plenum chamber, denoted as antechamber. The concept of a plenum chamber for homogenisation is well known in fluid mechanics (Guha, 2010) and rules of thumb exist to achieve good mixing and thus homogenisation using a large volume, many baffles and the longest possible distance in the antechamber. Hence, the antechamber is designed as a meandering structure, which makes good use of the given volume, has a long distance and sharp deflections at the bending, thus leading to homogeneous flow around the capillary.

Downstream of the mixing a nozzle follows in which the ink droplets are aerodynamically focused. Due to the aerosol generation inside of the mixing chamber, discontinuous operation is possible and thus enables the feature of AoD printing.

For manufacturing of a functional model of the aerosol print head for future use in a laboratory setup, a lathing process is available at our institute. Lathing is a process well suited to manufacture the almost completely rotationally symmetrical geometry of the print head. Also, surfaces with sufficiently low roughness can be achieved by lathing. The application of the lathing process results in a number of requirements which must be taken into account in the design of the print head. For example, the shallow angles required for aerodynamic focusing cannot be produced with the conventional lathing tool due to its limited insertion depth. This leads to a separation of the nozzle geometry into two sections: One with a nozzle angle of  $\alpha_1 = 45^\circ$ , which can be produced with the standard lathing tool, and a tip with a nozzle angle of  $\alpha_2 = 15^\circ$ , which is used for focusing the aerosol. This tip is manufactured with a conical milling tool. The minimum diameter of the nozzle exit, which can be manufactured with the conical milling tool, is 1 mm. The design parameters resulting from the process limitations are summarised in Table 1.

Table 1: Design parameters of the fabrication process.

Parameter	Value
Nozzle angle $\alpha_1$ [°]	45
Nozzle angle $\alpha_2$ [°]	15
Nozzle exit diameter $d$ [mm]	1

As material for the print head, the aluminum alloy AlMgSi1 is selected. These are the boundary conditions resulting from the fabrication processes used to be considered in geometrical modelling of the print head.

## 3 MODELLING

Modelling of the AoD-print head is on the basis of CFD, a numerical technique used to solve fluid mechanical problems. We are using Ansys Fluent in the versions R19.3 and R20.1 as CFD tool.

### 3.1 Theory

Our chosen modelling approach also takes turbulent flows into account. In principle, turbulence is described by the Navier-Stokes equations. However, a direct numerical simulation based on the Navier-

Stokes equations is not possible in most cases and averaging techniques are used to filter out all or at least parts of the turbulent spectrum (Ansys 2021). Ansys Fluent offers a large number of different turbulence models, none of which can be regarded as universally valid. For the work presented, we have used the Reynolds-averaged Navier-Stokes equations (Eqs. 1, 2).

$$\frac{\partial \rho}{\partial t} + \frac{\partial}{\partial x_i}(\rho u_i) = 0 \quad (1)$$

$$\begin{aligned} \frac{\partial}{\partial t}(\rho u_i) + \frac{\partial}{\partial x_j}(\rho u_i u_j) = \\ -\frac{\partial p}{\partial x_i} + \frac{\partial}{\partial x_j} \left[ \mu \left( \frac{\partial u_i}{\partial x_j} + \frac{\partial u_j}{\partial x_i} - \frac{2}{3} \delta_{ij} \frac{\partial u_k}{\partial x_k} \right) \right] + \\ \frac{\partial}{\partial x_j}(-\rho \overline{u_i u_j'}) \end{aligned} \quad (2)$$

Eq. 1 is the continuity equation, describing the conservation of mass where  $\rho$  is the density and  $u_i$  is the mean velocity. The conservation of momentum is represented by Eq. 2 where  $p$  is the static pressure and the symbol  $\delta_{ij}$  denotes the Kronecker-Delta. The Reynolds-averaged Navier-Stokes equations are generally favourable in terms of computational effort and time and are thus very well suited for the calculation of complex turbulent flows (Ansys 2021). By eliminating all turbulent structures from the flow, a uniform flow of the averaged velocity and pressure fields is achieved. Based on the Reynolds-averaged Navier-Stokes equations a large variety of engineering applications can be modeled. For our approach, we use the  $k$ - $\omega$ - $SST$  model (shear stress transport) which is a compressible turbulence model. Here, two additional transport equations are solved, one for the turbulence kinetic energy  $k$  (Eq. 3) and one for the specific dissipation rate  $\omega$  (Eq. 4).

$$\frac{\partial}{\partial t}(\rho k) + \frac{\partial}{\partial x_i}(\rho k u_i) = \frac{\partial}{\partial x_j} \left( \Gamma_k \frac{\partial k}{\partial x_j} \right) + G_k - Y_k + S_k \quad (3)$$

$$\begin{aligned} \frac{\partial}{\partial t}(\rho \omega) + \frac{\partial}{\partial x_i}(\rho \omega u_i) = \\ \frac{\partial}{\partial x_j} \left( \Gamma_\omega \frac{\partial \omega}{\partial x_j} \right) + G_\omega - Y_\omega + D_\omega + S_\omega \end{aligned} \quad (4)$$

With  $G_k$  representing the production of turbulence kinetic energy  $k$  and  $G_\omega$  the generation of the specific dissipation rate  $\omega$ .  $\Gamma_k$  and  $\Gamma_\omega$  give the effective diffusivity of  $k$  and  $\omega$ , respectively, while  $Y_k$  and  $Y_\omega$  imply the dissipation of  $k$  and  $\omega$  due to turbulence.  $D_\omega$  is the cross-diffusion term,  $S_k$  and  $S_\omega$  are user-defined sources, respectively. Detailed information of the calculation of this parameter can be found in Wilcox (2006) and Menter (1994).

The main advantage of the  $k$ - $\omega$  model is that the boundary layers are also modelled thus leading to

better results near the walls. In addition, on the basis of  $k$ - $\omega$  models boundary layer flows with unfavourable pressure gradient and dissipation can be better predicted. In the  $k$ - $\omega$  models of the  $SST$ , elements of the  $\omega$ -equation and the  $\varepsilon$ -equation are combined to avoid the sensitivity with respect to free flow inherent to the standard  $k$ - $\omega$  model. Furthermore, the  $SST$  model is calibrated to accurately calculate flow separation from smooth surfaces.

Modelling of the aerosol takes place with respect to the Euler-Lagrange consideration as discrete phases. In the Discrete Phase Model the droplet tracks are calculated inside of the velocity field of the continuous phase. The Euler-Lagrange approach neglects particle-particle interactions, and this requires that the discrete phase occupies only a low volume fraction (Ansys 2021). Since we estimate a volume fraction of the discrete phase of less than 10% of the total volume, the Euler-Lagrange consideration is well suited for efficient calculation of the individual droplets due to the small total number of droplets per volume fraction. The source characteristic of the aerosol generation is modelled using the cone injection model of Ansys Fluent which describes a conic-shaped particle injection for the aerosol where the following input parameters are available: Origin, particle distribution, temperature, cone axis, aerosol velocity, cone angle, particle diameter, mass flow, and the azimuth. The properties set in the model are shown in Tab. 2.

Table 2: Injection properties.

Parameter	Value
x-Position	[m] 0
y- Position	[m] 0
z- Position	[m] 0
Particle distribution	uniform
Particle diameter	[m] $2 \cdot 10^{-5}$
Temperature	[K] 300
Cone axis	(1/0/0)
Cone angle	[°] 25
Azimuthal start angle	[°] 0
Azimuthal stop angle	[°] 360
Velocity magnitude	[m/s] 10
Mass flow	[kg/s] parameter

### 3.2 Geometry

The geometry model must strictly follow the conditions and design rules of the manufacturing processes as defined in Section 2 and summarised in Tab. 1. Geometry parameters, which do not have a direct impact on the focussing of the aerosol jet, as long as they are within specific boundaries, are:

- dimensions of the mixing chamber and
- position and angle of the influx channel.

Length and width of the mixing chamber can be freely chosen, as long as they are sufficiently large to avoid a wetting of the inner walls by insufficient focussing. Manufacturing restriction on the other hand would prefer a short and compact design – these contradictory requirements must be well balanced and validated by simulations.

With respect to the inlet channel of the antechamber, free parameters are positioning and inlet-angle. The momentum transfer between aerosol and sheath gas depends on the vectorial difference of the velocities, i.e. focusing of the aerosol jet can be achieved on the one hand by a higher absolute difference in the velocities and on the other hand by different flow directions. The highest deflection of the aerosol is achieved by a sheath gas flow perpendicular to the droplet tracks. This can be obtained by placing the influx channel in the center of the mixing chamber at the height of the capillary tip. This positioning will cause eddies. To achieve an even, eddy-free flow in the mixing chamber the influx channel should be placed ahead of the capillary tip in flow direction. Furthermore a sharp edged transition from channel to chamber must be avoided, since again such a geometrical feature would cause eddies. For those reasons the inlet channel from the antechamber to the mixing chamber is tilted by an angle of  $60^\circ$  with respect to the cylindrical chamber wall. This will result in an eddy-free flow of the sheath gas around the capillary. Figure 2 shows the geometry model of the print head.

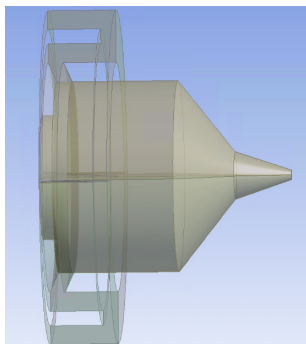


Figure 2: Geometry model of the print head.

### 3.3 Meshing

The result of a CFD simulation depends not only on how dense the mesh is in the area of large velocity gradients (e.g. on the walls) but also on the type of elements and symmetries in the meshes (see Fig. 3).

Interfaces that are not perpendicular to the largest mass flows (Fig.3, left) enhance numerical diffusion.

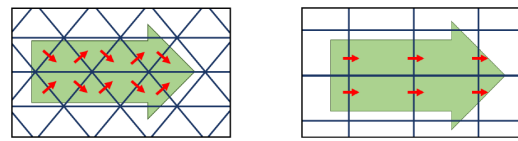


Figure 3: Mass flow in different meshes. Physical flow direction through the model (green) and flow through the interfaces of the elements (red).

Particularly critical areas with respect to meshing are the nozzle and the free jet. In the conical region of the nozzle, the element size decreases with the nozzle diameter. Thus, the mass flow through successive elements remains approximately the same, which reduces numerical diffusion. In this case, usage of a tetrahedral mesh is appropriate (see Fig. 4, left, dashed frame). In the transition zone between nozzle and free jet at the tip of the nozzle, a transfer from tetrahedral elements to hexahedral elements is implemented (see Fig. 4, center, solid ellipse).

A free jet does not always have a unique, mathematically stable solution, so numerical diffusion must be minimised to improve convergence. This is achieved by selecting the mesh in such a way that the boundary surfaces of the elements are as perpendicular as possible to the largest mass flows (see Fig. 4, right, solid frame). This would not be the case for elements in tetrahedral form or asymmetric meshes. Here the generation of asymmetric solutions due to numerical diffusion are more likely.

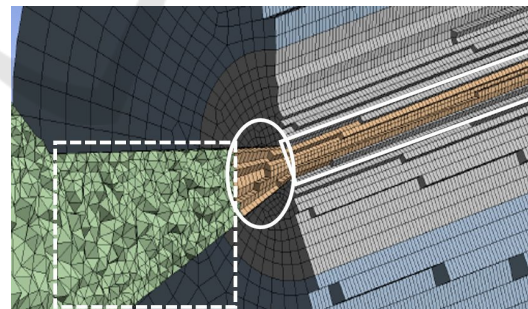


Figure 4: Section through the mesh used; decreasing element size in the area of the nozzle (left, dashed frame), symmetrical meshing in the area of the free jet (right, solid frame) and transition zone (middle, solid ellipse).

In turbulent flows, special attention must be paid to the boundary conditions at the walls, since different layers form here. The transition from the fully turbulent to the wall can be divided into three layers: the purely viscous bottom layer, the transition layer and the overlap layer (Schlichting and Gersten 2006).

The  $k-\omega$ - $SST$ -model used also models the boundary layers and requires a much finer meshing at the wall. Comparability of the boundary layers in different flows is achieved by the de-dimensioned wall distance (Eq. 5).

$$y^+ = \rho u_\tau \frac{y}{\mu} \quad (5)$$

with  $u_\tau = \sqrt{\frac{\tau}{\rho}}$ .

Here  $\rho$  denotes the density,  $u_\tau$  the shear stress rate,  $\mu$  the viscosity, and  $\tau$  the shear stress in that layer. The required resolution of the meshing thus depends on both the choice of turbulence model and the velocity gradients due to the de-dimensioned wall spacing (Ansys 2021). This means that for the same geometry and different flow velocities, different densities of meshing must be chosen.

In our model, the wall layers are meshed at a very fine resolution, so that the first mesh element is in the range  $y^+ \approx 1$ . Thus, the influences of the purely viscous sublayer are fully represented (Ansys 2021). This resolution is achieved by using prism elements in this layers.

Furthermore, since the Euler-Lagrange model used involves a particle-related consideration of the discrete phase, it must be ensured that in principle a particle can be located completely within a mesh element. Therefore, care must be taken that the minimum size of the mesh elements is chosen in a way that it reaches a multiple of the particle size. The mesh consists of 4,107,235 elements with 1,097,103 nodes and a minimum edge length of 60  $\mu\text{m}$ . Generation of the prism layers is conducted with a transition rate of 0.272 and a growth rate of 1.2.

## 4 SIMULATION

The simulation is carried out on a workstation. The processor used is the AMD Ryzen Threadripper 3970X with 32 cores, 64 threads at 3.7 GHz, 128 GB RAM and an Nvidia Titan RTX graphics processor with 24 GB.

### 4.1 Modelling of Ink and Sheath Gas

The ink is modelled as distilled water so that the discrete phase consists of atomised droplets. Replacing the functional ink with distilled water in the model is permissible because aerodynamic focusing does not depend on the dynamic viscosity of the ink or the particle content in the ink. Hence, once the simulative functional proof of aerodynamic focusing has been provided, it is basically possible for

all liquids that can be atomised in the capillary. If the droplets of functional inks have a different momentum than the droplets of distilled water due to their density or diameter, the sheath gas mass flow can be adjusted in such a way that focusing of the aerosol jet is achieved.

The droplets make up only a small volume fraction in the mixing chamber ( $< 10\%$  of the total volume), thus the particle-particle interaction of the droplets can be neglected. However, a coupling of the discrete phase with the continuous phase is established so that a momentum transfer of the aerosol to the sheath gas, which is not negligible for large aerosol mass flows, is taken into account. Table 3 shows the simulation parameter of the aerosol at the outlet of the capillary (Zeltner 2020).

Table 3: Simulation parameters of the aerosol at the outlet of the capillary.

Parameter	Value
max. exit angle [°]	25
max. diameter of droplets [ $\mu\text{m}$ ]	20
max. exit velocity [m/s]	10
max. aerosol mass flow [kg/s]	$1.21 \cdot 10^{-5}$

The sheath gas is the continuous phase in the Discrete Phase Model. As sheath gas Argon is modelled as an ideal gas. The parameters are depicted in Table 4.

Table 4: Modelled properties of Argon.

Parameter	Value
Specific heat [J/(kg K)]	520.64
Thermal conductivity [W/(m K)]	0.0158
Viscosity [kg/(m s)]	$2.125 \cdot 10^{-5}$
Molecular weight [kg/kmol]	39.948

### 4.2 Determination of the Operating Point

Based on the modelling of the entire print head, simulations of the printing process are carried out. In the first step, the operating points are determined at which the aerosol can be focused by means of the sheath gas without contact with the wall. To determine these working points, the mass flow of the sheath gas is changed step by step for varying mass flows of the aerosol until no contact of the aerosol with the nozzle walls occurs.

Figure 5 shows the relationship between sheath gas mass flow, aerosol mass flow, and wall contact. The red diamonds depict mass flow combinations resulting in a wall contact, while blue dots denote mass flow combinations without wall contact. The

region of operation without wall contact can be separated by a straight line from the region with wall contact.

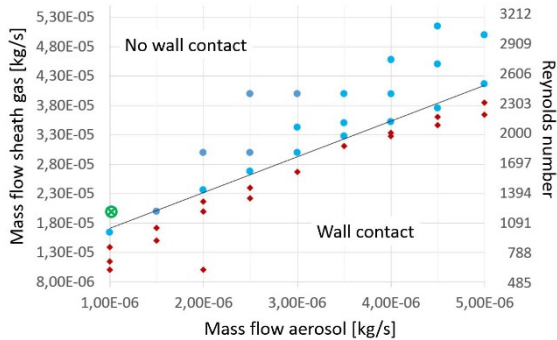


Figure 5: Relationship between sheath gas mass flow and aerosol mass flow. Blue dots: no wall contact; red diamonds: wall contact; green encircled cross: chosen operating point.

Since the Reynolds number is linearly dependent on the sheath gas mass flow, it is also possible to directly infer the Reynolds number for the process window. With the help of the diagram in Fig. 5, it is possible to determine a maximum aerosol mass flow at a specified sheath gas mass flow. For proper operation of the nozzle, a laminar flow of the ink is required. The operating point of the nozzle is therefore selected to achieve a low Reynolds number to allow for laminar flow. Hence, an operating point at a Reynolds number of  $Re = 1200$  is chosen for the further simulations, which corresponds to a sheath gas mass flow of  $2 \cdot 10^{-5}$  kg/s. If the momentum of the aerosol mass flow is too large, eddies will form due to mass conservation, which will deflect some of the droplets towards the nozzle wall (Fig. 6 b).

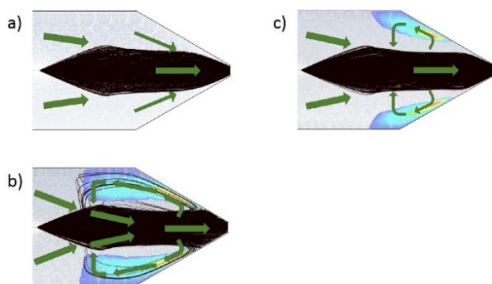


Figure 6: Eddy generation in the nozzle at  $Re = 1200$  and increasing aerosol mass flow. Droplet tracks (black) and flow of the sheath gas (green). a): no wall contact, aerosol mass flow  $1 \cdot 10^{-6}$  kg/s; b): light wall contact, aerosol mass flow  $2 \cdot 10^{-6}$  kg/s; c): strong wall contact, aerosol mass flow  $5 \cdot 10^{-6}$  kg/s.

Furthermore, if the aerosol mass flow is too large, the aerosol cannot be deflected sufficiently towards the axis of symmetry, so that wetting of the nozzle walls occurs (Fig. 6 c). If the mass flows are in the range above the straight line of Fig. 5, no eddies form and the aerodynamic focusing is large enough to prevent wetting of the nozzle walls (Fig. 6 a). Hence, the operating point is specified with a sheath gas mass flow of  $2 \cdot 10^{-5}$  kg/s ( $Re = 1200$ ) and an aerosol mass flow of  $1 \cdot 10^{-6}$  kg/s (marked by the green encircled cross in Fig. 5) to ensure an operating point with no wall contact.

### 4.3 Steady-state and Transient Considerations

As the operating point of the print head has been determined, the functionality of the printing process can be examined. The free jet is included in the investigations, as the focusing of the jet outside the nozzle is to be examined. At the boundary of the control space, a constant pressure to the environment is set as a boundary condition. Inflow and outflow is allowed for all modeled phases (pressure outlet). Figure 7 shows the static pressure distribution for the model used.

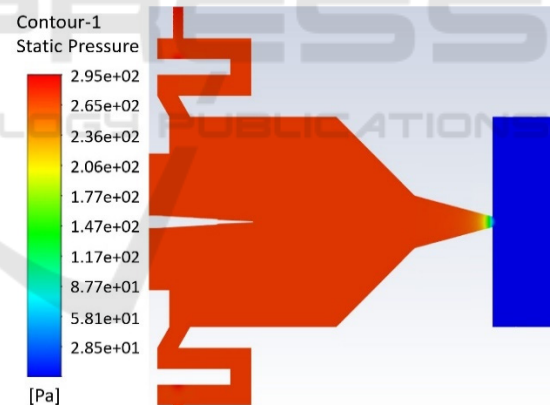


Figure 7: Static pressure.

In order to deliver reproducible results, a time-independent, i.e. steady, behaviour of the printing process is necessary. Therefore, steady-state simulations are carried out first. The settings listed in Tables 3 and 4 are used for this purpose. Results of the steady-state simulations at the operating point are a focussed aerosol jet with a diameter of approx. 0.8 mm when leaving the nozzle and approx. 0.15 mm at the focal point, located at a distance of 4.2 mm from the nozzle (Fig. 8 b). In the nozzle no wall contact occurs and the flows are rotationally symmetrical.

Hence, in steady-state, the proper functioning of the AoD print head is validated by simulation.

Time-resolved transient simulations are also performed to investigate whether truly stable steady-state solutions are present or whether they are merely averages of a transient solution.

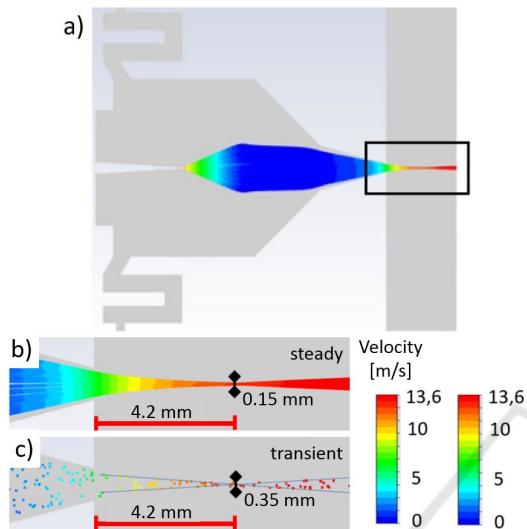


Figure 8: Simulation of the droplet tracks for the entire system. The rectangular region in a) is the region of interest. b) steady-state simulation, c) transient simulation.

Due to the transient observation, another particle model has to be used, which is called *unsteady particle tracking* in Ansys Fluent. In this particle model, individual droplets have a position and a velocity in every time step. No continuous trajectories are calculated, but only the position of the droplets is updated. The number of newly generated droplets per time step is set to 20 to limit the computational effort. A very fine time increment is necessary for the droplets after they leave the capillary. The fine time increment leads to extremely slow movements of the droplets elsewhere in the model, so that in the simulation over 1000 time increments are necessary until a steady aerosol flow reaches the substrate. This makes the time-resolved simulations very computationally intensive. The required time increment for the droplets was set at 0.1 ms per increment. The total simulated time span is approx. 0.5 s.

The time-resolved simulations give similar results to the steady-state simulations (see Fig. 8 c). Again, no wall contact occurs in the nozzle. The position of the focal point and the velocities of the droplets are identical in both approaches (see Fig. 8 and Table 5).

However, the diameter of the focal point is larger in the transient simulations than in the steady-state

simulations. A deflection or defocusing of the aerosol jet due to turbulence in the free jet is neither observed in the steady-state nor in the time-resolved simulations.

As a result, it can be stated that steady-state solutions form at the free jet. These results confirm the assumption of a steady-state behaviour, which is of existential importance for functional printing.

Thus, all requirements for AoD-printing are fulfilled and the newly developed concept has been validated by simulation.

Table 5: Properties of steady and transient simulations.

Property	steady	transient
Reynolds number	1200	1200
max. velocity sheath gas	18.3 m/s	18.3 m/s
max. velocity droplets	13.6 m/s	13.6 m/s
velocity droplets @ nozzle exit	7 m/s	7 m/s
Diameter aerosol jet @ nozzle exit	0.8 mm	0.9 mm
Diameter aerosol jet @ focus	0.15 mm	0.35 mm
focus position	4.2 mm	4.2 mm

## 5 CONCLUSIONS

In this article we present the proof-of-concept of a new principle of an aerosol jet-on-demand print head for functional printing by means of CFD simulations. Aerodynamic focusing of the aerosol jet is based on properly adjusting the mass flows of the sheath gas and the aerosol and the appropriate design of the outlet nozzle. Design considerations are made with respect to generation of a homogenised sheath gas flow and the manufacturing processes available at our institute, thus resulting in a design-for-manufacturing approach. Modelling and meshing of the print head is discussed for the critical areas to avoid numerical diffusion and to improve the convergence.

Simulation of the operation of the print head is done by modelling the functional ink as distilled water. Since aerodynamic focusing is independent of the dynamic viscosity of the fluid or the particle content in the fluid, this approach is permissible. In principle, aerodynamic focusing of all fluids that can be atomised in the capillary is possible. If, due to density or diameter, the droplets of functional inks have a different momentum than the droplets of distilled water, the mass flows of the sheath gas and the aerosol have to be adjusted to achieve focusing of the aerosol jet.

There are two conditions which must be met for reliable function of the aerosol jet-on-demand print

head. These are on the one hand the generation of a stable and focused aerosol beam, and on the other hand the prevention of wetting of the inner nozzle wall by the aerosol. The fundamental operating parameters ensuring these conditions are found by CFD simulations. In a first step the relationship between the mass flows of the sheath gas and the aerosol and the wetting of the inner wall is investigated leading to an operating point at  $Re = 1200$  ensuring a non-wetting condition. Since a time-continuous operation of the print head is a prerequisite of a reliable function of aerosol-on-demand printing, steady-state as well as transient simulations are performed to investigate for time dependency of the solutions. The transient simulations give identical results as the steady-state simulations concerning the position of the beam focus as well as the velocity distribution. Thus, all requirements for aerosol-on-demand printing are fulfilled and the newly developed concept has been validated by simulation. In future studies, the simulative findings will be experimentally evaluated and validated by realising the design-for-manufacture as experimental setup.

## REFERENCES

- Ansyz 2021. *Ansyz Fluent User's Guide, Release 2021 R2*, ANSYS, Inc. Canonsburg, PA, USA
- Chang, J.S., A.F. Facchetti, and R. Reuss. 2017. A circuits and systems perspective of organic/printed electronics: Review, challenges, and contemporary and emerging design approaches. *IEEE Journal on emerging and selected topics in circuits and systems* 7, : 1–21. doi: 10.1109/JETCAS.2017.2673863.
- Ganz, S., H.M. Sauer, S. Weißenseel, J. Zembron, R. Tone, E. Dörsam, M. Schaefer, M. Schulz-Ruthenberg. 2016. *Printing and Processing Techniques*. Nisato, G., Lupo, D., and Ganz, S. (editors): *Organic and Printed Electronics: Fundamentals and Applications*: 48-116. Singapore: Pan Stanford Publishing.
- Gupta, A.A., A. Bolduc, S. G. Cloutier and R. Izquierdo. 2016. Aerosol Jet Printing for printed electronics rapid prototyping, *IEEE International Symposium on Circuits and Systems (ISCAS), Montreal, QC*: 866-869, doi: 10.1109/ISCAS.2016.7527378.
- Guha, A. and Smiley, B. 2010. Experiment and analysis for an improved design of the inlet and nozzle in Tesla disc turbines. *Proceedings of The Institution of Mechanical Engineers Part A-journal of Power and Energy - PROC INST MECH ENG A-J POWER* 224. doi: 10.1243/09576509JPE818.
- Hedges, M. and A. B. Marin. 3D Aerosol Jet Printing - Adding Electronics Functionality to RP/AM. *Direct Digital Manufacturing Conference (Berlin) 2012*. url: [https://optomec.com/wp-content/uploads/2014/04/Optomec\\_NEOTECH\\_DDMC\\_3D\\_Aerosol\\_Jet\\_Printing.pdf](https://optomec.com/wp-content/uploads/2014/04/Optomec_NEOTECH_DDMC_3D_Aerosol_Jet_Printing.pdf). (accessed: 24.02.2020).
- Magdassi, S. 2010. *The Chemistry of Inkjet Inks*. Singapore: World Scientific Publishing.
- Menter, F.R. 1994. Two-Equation Eddy-Viscosity Turbulence Models for Engineering Applications. *AIAA Journal*. 32(8): 1598–1605.
- Mette, A., P. L. Richter, M. Hörteis, S. W. Glunz. 2007. Metal Aerosol Jet Printing for Solar Cell Metallization, *Progress in Photovoltaics* 15, 621–627. doi: 10.1002/ppp.759.
- Neotech. 2021. 3D Printed Electronics applications realised by Neotech AMT. url: <https://neotech-amt.com/applications>. (accessed: 19.10.2021).
- Schlichting, H. and K. Gersten. 2006. *Grenzschichttheorie*. 10. Auflage. Berlin, Heidelberg: Springer. doi: 10.1007/3-540-32985-4.
- Sieber, I. R. Thelen, and U. Gengenbach. 2020. Assessment of high-resolution 3D printed optics for the use case of rotation optics. *Opt. Express* 28: 13423-13431.
- Sieber, I., R. Thelen, and U. Gengenbach. 2021. Enhancement of High-Resolution 3D Inkjet-printing of Optical Freeform Surfaces Using Digital Twins. *Micromachines* 12(1): 35. <https://doi.org/10.3390/mi12010035>.
- Sieber, I., Zeltner, D., Ungerer, M., Wenka, A., Walter, T., Gengenbach, U. (2022). Design and experimental setup of a new concept of an aerosol-on-demand print head. *Aerosol Science and Technology*. Taylor & Francis. DOI: 10.1080/02786826.2021.2022094
- Sirringhaus, H. and T. Shimoda. 2003. Inkjet Printing of Functional Materials. *MRS Bulletin* 28(11): 802–806. doi: 10.1557/mrs2003.228.
- Wilcox, D.C. 2006. *Turbulenc Modelling for CFD*, 3rd edition). La Canada, California: DCW Industries, Inc.
- Ungerer, M., A. Hofmann, R. Scharnowell, U. Gengenbach, I. Sieber, and A. Wenka. 2018. Druckkopf und Druckverfahren [Print head and printing method]. Patent: DE 10 2018 103 049.5.
- Ungerer, M. 2020. Neue Methodik zur Optimierung von Druckverfahren für die Herstellung funktionaler Mikrostrukturen und hybrider elektronischer Schaltungen [New methodology for optimising printing processes for the production of functional microstructures and hybrid electronic circuits]. Dissertation, Karlsruhe, Germany: Karlsruhe Institute of Technology (KIT).
- Zeltner, D. 2020. Auslegung und Evaluierung einer Dosiereinheit zur additive Fertigung funktionaler Strukturen [Design and evaluation of a dispensing unit for additive manufacturing of functional structures]. Karlsruhe: Karlsruhe Institute of Technology, Institute for Automation and Applied Informatics.